Showcasing research from Professor Jingwei Hou's laboratory, School of Chemical Engineering, University of Queensland, St Lucia, Australia.

Aggregation suppression and enhanced blue emission of perylene in zinc-based coordination polymer glass

Blue-emitting coordination polymer glasses were fabricated using perylene dye and a zinc-based coordination glass. Solid-state aggregation-caused quenching (ACQ) of perylene monomers was significantly suppressed, yielding a stable hybrid glass with a high photoluminescent quantum yield of 75.5%.

ROYAL SOCIETY
OF **CHEMISTRY**

rsc.li/chemcomm

ChemComm

Check for updates

Aggregation suppression and enhanced blue emission of perylene in zinc-based coordination polymer glass†

Jaeho Lee,[a] Zixi Xie,*[a] Wengang Huang,[a] Milton Chai, [ID][a] Xuemei Li, [ID][a] Bun Chan, [ID][b] Huiyuan Cheng,[c] Dongxu He,[c] EQ Han,[a] Yuelei Chen,[a] Vicki Chen, [ID][d] Lianzhou Wang [ID][ac] and Jingwei Hou [ID]*[a]

Reducing aggregation caused quenching and enhancing stability is crucial in the fabrication of organic light-emitting diodes. Herein, we successfully fabricated blue-emitting coordination polymer glasses using perylene dye and a zinc-based coordination glass. The aggregation of perylene monomers in the solid state was significantly suppressed, and the hybrid glass demonstrated high stability and strong photoluminescent quantum yield (75.5%) under ambient conditions.

High-efficiency and operationally stable blue-emitting organic light-emitting diodes (OLEDs) are essential for solid-state lighting applications.[1,2] Some of the most studied materials for blue emission are noble metal-based phosphors such as iridium, platinum, and ruthenium given their high light emitting efficiency. However, their low stability, coupled with the high cost of noble metals, makes all-organic dyes a promising alternative for fabricating emitting diodes.[3] Perylene, one of the most investigated organic dyes, is renowned for its excellent chemical, thermal, and optical stabilities, as well as its high luminescence efficiency. While perylene demonstrates excellent photoluminescence quantum yield (PLQY) with blue emission in solvents like tetrahydrofuran, its efficiency remarkably decreases and photoluminescence emission peak redshifts in the solid-state form due to aggregation caused quenching (ACQ). This is due to the material's tendency to form aggregated stacks in the solid state, facilitated by intermolecular π–π interactions.[4,5]

To mitigate these effects, several approaches have been explored, including embedding perylene in a host matrix or introducing long-chain organic substitutions on chromophores to minimize intermolecular interactions between individual perylene monomers, thereby reducing aggregation.[6] However, the strong tendency for π–π stacking of the fluorescent monomers either complicates the process of substituting long alkyl chains onto the chromophores or lowers efficiency compared to its liquid form, leading to significant challenges for practical implementations of the material in OLED applications.[7,8]

Coordination polymers (CPs) are organic–inorganic hybrid materials that have coordination bonds with extended networks. Due to their high tunability in structures and chemical compositions, CPs possess diverse chemical and physical properties, making them strong candidates for various applications such as gas separation, protective matrices, molecular storage, sensors, proton conductors and LEDs.[9,10] One recent advancement in this field is coordination polymer glass, which has an amorphous structure and a viscous flowing state when heated above its glassy transition temperature (T_g). This glassy phase has attracted considerable attention due to its ability to overcome certain intrinsic limitations of the crystalline phase, such as controlling grain boundaries, processibility and limited mechanical properties, opening up various potential applications in electrochemical, photovoltaic, and OLED technologies.[11–13]

The glassy materials also open great opportunities for composite formation and engineering: the viscous flowing materials render a solvent-like environment that facilitates the dispersion of secondary components with highly tuneable interfacial properties, which can be maintained even after the solid glassy phase forms. In this work, a zinc-based CP glass containing benzimidazole (bIm) and protic ionic liquid (benzimidazole)($H_2PO_4^-$) is synthesized in crystal form (Zn–P–bIm) and then explored as a host glassy matrix (a_gZn–P–bIm, where a_g represents the amorphization by glassy formation) for solid-state perylene composite. Among the various coordination polymer glasses, Zn–P–bIm was selected due to its low absorption in the visible light region in its glass form and its relatively low melting point, which minimizes the risk of thermal decomposition of perylene during

[a] School of Chemical Engineering, University of Queensland, St Lucia, Queensland 4072, Australia. E-mail: jingwei.hou@uq.edu.au

[b] Graduate School of Engineering, Nagasaki University, Nagasa-ki, 852-8521, Japan

[c] Australian Institute for Bioengineering and Nanotechnology, The University of Queensland, St Lucia, QLD, 4072, Australia

[d] University of Technology Sydney, Ultimo, NSW, 2007, Australia

composite formation, making it suitable for applications requiring blue-emitting glass.[14,15] The hybrid glassy composite features strong blue photoluminescence, indicating successful encapsulation of perylene in a solid state without significant undesirable ACQ phenomenon. This development paves the way for more efficient and stable blue-emitting glass in OLED applications.

As a host matrix, Zn–P–bIm was synthesized *via* a mechanochemical process using zinc acetate, bIm, and phosphoric acid. The prepared crystals were then melted on a hot plate at 130 °C and cooled at ambient temperature to form an amorphous glass (a_gZn–P–bIm). For the perylene hybrid composite, the Zn–P–bIm crystal powder was mixed with 0.5 wt% perylene before undergoing the same melting procedure at 130 °C followed by cooling. The powder mixture is referred to as P–Zn–P–bIm, and when it transitions to the glass phase through the melting, it is denoted as P–a_gZn–P–bIm.

Differential scanning calorimetry (DSC) was conducted to understand the melting process and thermal behavior of the material upon heating and compositing. The melting temperature of the perylene-containing Zn–P–bIm was found to be slightly lower than that of pure Zn–P–bIm, suggesting effective interfacial interaction occurred through mixing, leading a slightly higher entropy terms for the Zn–P–bIm phase (Fig. S1, ESI†).[16] Photoluminescent spectroscopy analysis showed that pure perylene exhibits aggregation caused quenching (ACQ) due to π–π stacking in the solid state at ambient conditions, resulting in a broad and weak emission peak at 590 nm.[17] The pure a_gZn–P–bIm materials displayed no photoluminescence under the same excitation conditions. Interestingly, the composite P–a_gZn–P–bIm exhibited a noticeable blue PL emission with two distinct peaks at 458 and 480 nm, a phenomenon mostly only seen in perylene in solution (Fig. S2, ESI†).[18] This indicates that aggregation has been effectively suppressed by the glass matrix, resulting in a noticeable blue shift and strong photoluminescence. Upon heating, the Zn–P–bIm formed a transparent glass with no visible emission under UV light. In contrast, the perylene hybrid composite became a semi-transparent glass with a slight yellow color under bright field and blue photoluminescent behavior when excited under UV light (Fig. 1 and Fig. S3a, b, ESI†).

Additionally, the P–Zn–P–bIm exhibits a weak PL peak near 590 nm due to the low loading of perylene in the mixture. However, upon forming the glass composite, the peak shifts and intensifies significantly. Furthermore, UV-vis spectroscopy reveals that the composite exhibits an absorption trend similar to perylene, distinctly differing from that of a_gZn–P–bIm (Fig. S4, ESI†). The photoluminescence quantum yield (PLQY) analysis of this hybrid composite showed a 75.5% quantum yield with CIE color coordinates at (0.15, 0.28), a noteworthy improvement in the PL of perylene in the solid state, as the PLQY of the pure phase was measured at 13.95% (Fig. S5, ESI†). Notably, before undergoing the melting process, P–Zn–P–bIm exhibited no PL emission, similar to a_gZn–P–bIm.

Furthermore, time-resolved photoluminescence (TRPL) spectroscopy on nanosecond time scale was conducted to investigate ex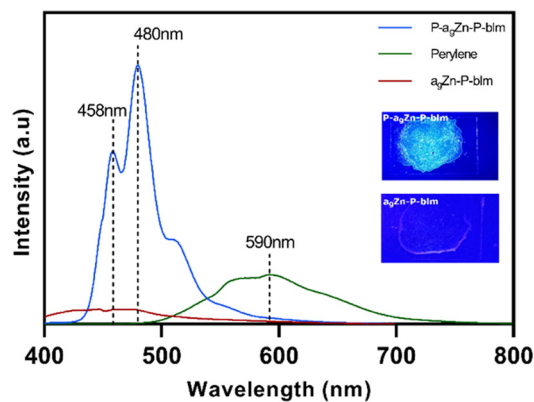cited charge carrier recombination in the hybrid composite system. The TRPL decays showed that the perylene crystals in the solid state had a longer decaying tail compared to the hybrid system. Considering the short lifetime of a_gZn–P–bIm, which is not photoactive, the shorter lifetime observed in the perylene composite glass compared to its pure phase can be attributed to interactions between the glass matrix and the perylene (Fig. S6, ESI†).[19]

To understand the noticeable improvement in PL of the hybrid material and the structure of the composite, wide-angle X-ray scattering (WAXS) was utilized. WAXS is a powerful tool for characterizing the arrangement of atoms and the degree of crystallinity in polymeric materials. In this study, WAXS revealed the clear crystallinity in the Zn–P–bIm crystals, which aligned well with the simulated structure (Fig. S7, ESI†). The crystalline structure transformed into an amorphous form upon melting and quenching, resulting in a glassy composite state where the self-assembly of perylene was effectively suppressed (Fig. 2a). We further analyzed the composite using phosphorus (^{31}P) solid-state nuclear magnetic resonance (SSNMR), to understand the atomic-level chemical structure. The spectrum of Zn–P–bIm shows two distinct phosphate peaks at −0.48 and 2.8 ppm, indicating the presence of phosphate diester and mono-coordination. This suggests that bIm and phosphoric acid participate in the coordination with zinc ions during the formation of Zn–P–bIm. Upon heating, these two peaks merge into one broad peak, aligning with the formation of an amorphous glassy structure. The perylene hybrid composite shows the development of a shoulder peak at ca. −6.7 ppm, indicating the formation of new chemical bonds between phosphate and perylene within the glass matrix (Fig. 2b).[20,21] Scanning electron microscopy (SEM) and 3D fluorescence microscopy were utilized to analyze the surface morphology and homogeneity of the hybrid composite (Fig. 2c and d), showing the surface of P–a_gZn–P–bIm composite becomes very smooth. Under fluorescence microscopy, the composite exhibits well-dispersed blue light emission with no visible solid grains at the submicron scale. This effective dispersion of perylene within the glass phase, along with the low material loading, likely explains
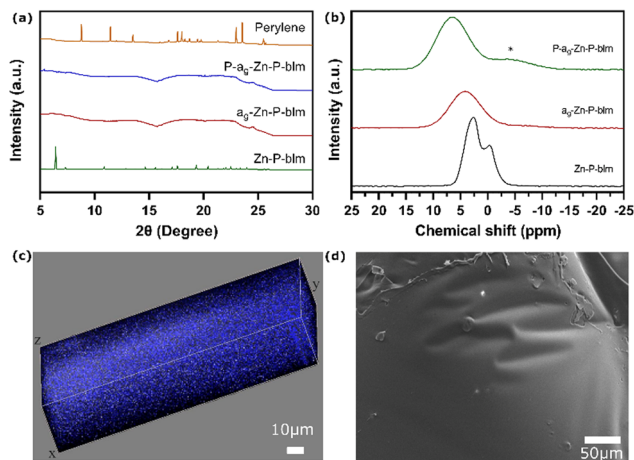

Fig. 1 Photoluminescence spectra perylene, a_gZn–P–bIm and P–a_gZn–P–bIm, along with photographs of P–a_gZn–P–bIm and a_gZn–P–bIm under 395 nm UV light. The PL spectra were recorded using 375 nm excitation, with all samples measured in the solid state under ambient conditions.

Fig. 2 (a) WAXS analysis of perylene, Zn–P–bIm, a_gZn–P–bIm and P–a_gZn–P–bIm composite, (b) phosphorus (^{31}P) SSNMR of Zn–P–bIm, a_gZn–P–bIm and P–a_gZn–P–bIm composite, * indicate the shoulder peak. Surface analysis of P–a_gZn–P–bIm using (c) 3D fluorescence microscopy images and (d) SEM with a secondary electron mode.

the absence of visible Bragg diffraction patterns in the WAXS measurements (Fig. 2a).

Synchrotron terahertz (THz) FarIR vibrational spectroscopy provides deeper insights into the interface properties of Zn–P–bIm and P-Zn–P–bIm composite. The peak at *ca.* 182 cm^{-1}, which can be assigned to the planer distortion of the perylene molecule based on the DFT calculation (Fig. S9, ESI†), shifted to a higher wavenumber after composting (Fig. 3). This result indicates the interfacial interaction suppresses the movement of the perylene molecules, indicating the potential formation of interaction bonds between the two phases. This result aligns with the findings from the ^{31}P SSNMR analysis, further supporting the hypothesis of PO$_4$ bonding with perylene in the composite structure.
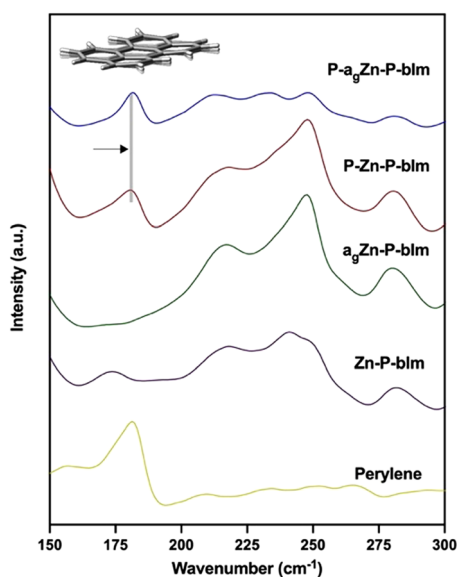

Fig. 3 THz-FarIR spectroscopy of perylene, Zn–P–bIm, a_gZn–P–bIm, P–Zn–P–bIm and P–a_gZn–P–bIm composite.

X-ray absorption spectroscopy (XAS) is a versatile tool to understand the oxidation state and atomic structure of material. The X-ray absorption near edge structure (XANES) spectra with the K-edge peak between 9600 and 10 000 eV provide the zinc coordination structure within the glass matrix.[22,23] It shows that the oxidation state of the a_gZn–P–bIm composite has zinc phosphate coordination. The reduction in P–a_gZn–P–bIm indicates the perylene within the matrix forming new coordination bond with phosphate. This leads to less coordination of zinc at the interfacial layer with perylene (Fig. S10, ESI†).[24] Furthermore, the fitting results of both k and r space from the extended X-ray absorption fine structure (EXAFS) indicate that the perylene-containing composite has a slightly lower Zn–O coordination number compared to a_gZn–P–bIm, with values of 1.41 for a_gZn–P–bIm and 1.27 for P–a_gZn–P–bIm while the Zn–N coordination number is higher at 2.59 and 2.73, respectively.

These results suggest that potential chemical bonds form between phosphate and perylene in the composite, leading to a partial replacement of oxygen from the phosphate surrounding the zinc ion with nitrogen (Fig. 4a, b and Table S1, S2, ESI†). X-ray photoelectron spectroscopy (XPS) was conducted to understand the surface chemical bonding of hybrid composite. P–a_gZn–P–bIm composite shows an increase of zinc 2p2 binding energy as well as phosphate p2p compared to a_gZn–P–bIm. These results also corroborate with the XAS results. (Fig. 4c, d and Fig. S11, ESI†).

Stability is a crucial performance parameter for emitting device applications, especially under ambient conditions.[25] The composite exhibited good stability for over a month storing under ambient conditions, retaining more than 90% of its initial photoluminescence, as shown in Fig. S12 (ESI†). The unexpected increase in PL intensity observed on day 35 is likely attributable to experimental variability, particularly due to the positioning of the sample during the test. It seems that the seamless integration of perylene within the glass matrix, combined with the chemical bonding between perylene and phosphate, effectively suppresses aggregation of monomer in the
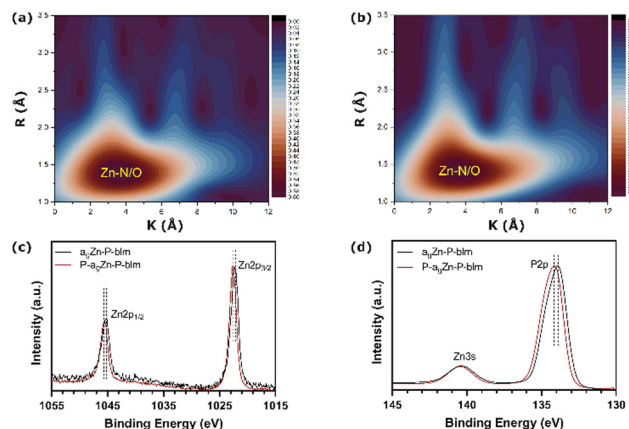

Fig. 4 XAS analysis, wavelet transform for the k_2-weighted Zn K-edge EXAFS signals of (a) a_gZn–P–bIm and (b) P–a_gZn–P–bIm composite. Interfacial chemical bonding analysis of P–a_gZn–P–bIm composite (c) phosphorus XPS and (d) zinc XPS.

solid state and enhances emission and the stability of the composite.[26]

In summary, the ACQ of perylene has been significantly suppressed within the polymer glass matrix, resulting in a composite glass with strong blue emission that remains highly stable under ambient conditions. Material characterization reveals that the primary mechanism for aggregation suppression is related to the formation of new chemical bonds between the phosphate within the glass network and perylene along with submicron level dispersion. Given its strong PLQY, stability and transparency, this approach could pave the way for developing semi-transparent hybrid composite glasses using other organic dye molecules facing similar challenges. In addition, the low toxicity and low viscosity of the materials make it suitable for scalable fabrication methods. For example, hot-casting the material into thin glass layers over appropriate substrates could enable large-scale manufacturing for various photonic applications such as LEDs and fluorescent logic gate.[27]

Data availability

The data supporting this article have been included as part of the ESI.†

Conflicts of interest

There are no conflicts to declare.

Notes and references

1 S. Izawa, M. Morimoto, K. Fujimoto, K. Banno, Y. Majima, M. Takahashi, S. Naka and M. Hiramoto, *Nat. Commun.*, 2023, **14**, 5494.
2 J. Lee, Z. Xie, L. Wang and J. Hou, *Chemistry*, 2024, **30**, e202400372.
3 H. Liu, Y. Fu, B. Z. Tang and Z. Zhao, *Nat. Commun.*, 2022, **13**, 5154.
4 F. Zhang, Y. Ma, Y. Chi, H. Yu, Y. Li, T. Jiang, X. Wei and J. Shi, *Sci. Rep.*, 2018, **8**, 8208–8211.
5 S. T. Wang, Y. J. Liu, C. C. Feng, W. H. Fang and J. Zhang, *Aggregate*, 2023, **4**, e264.
6 Y. Zou, V. Bonal, S. Moles Quintero, P. G. Boj, J. M. Villalvilla, J. A. Quintana, G. Li, S. Wu, Q. Jiang, Y. Ni, J. Casado, M. A. Díaz-García and J. Wu, *Angew. Chem.*, 2020, **132**, 15037–15044.
7 G. Boobalan, P. M. Imran, S. G. Ramkumar and S. Nagarajan, *J. Lumin.*, 2014, **146**, 387–393.
8 Z. Chen, U. Baumeister, C. Tschierske and F. Würthner, *Chem. – Eur. J.*, 2007, **13**, 450–465.
9 J. Li, J. Wang, Q. Li, M. Zhang, J. Li, C. Sun, S. Yuan, X. Feng and B. Wang, *Angew. Chem.*, 2021, **133**, 21474–21479.
10 T. Ogawa, K. Takahashi, S. S. Nagarkar, K. Ohara, Y.-L. Hong, Y. Nishiyama and S. Horike, *Chem. Sci.*, 2020, **11**, 5175–5181.
11 M. Ghasemi, X. Li, C. Tang, Q. Li, J. Lu, A. Du, J. Lee, D. Appadoo, L. H. G. Tizei, S. T. Pham, L. Wang, S. M. Collins, J. Hou, B. Jia and X. Wen, *Small*, 2023, **19**, e2304236.
12 J. Lee, L. Wang and J. Hou, *Microstructures*, 2023, **3**, 2023021.
13 X. Li, W. Huang, A. Krajnc, Y. Yang, A. Shukla, J. Lee, M. Ghasemi, I. Martens, B. Chan, D. Appadoo, P. Chen, X. Wen, J. A. Steele, H. G. Hackbarth, Q. Sun, G. Mali, R. Lin, N. M. Bedford, V. Chen, A. K. Cheetham, L. H. G. Tizei, S. M. Collins, L. Wang and J. Hou, *Nat. Commun.*, 2023, **14**, 7612.
14 D. Umeyama, S. Horike, M. Inukai, T. Itakura and S. Kitagawa, *J. Am. Chem. Soc.*, 2015, **137**, 864–870.
15 Z. Yu, L. Tang, N. Ma, S. Horike and W. Chen, *Coord. Chem. Rev.*, 2022, **469**, 214646.
16 J. Hou, P. Chen, A. Shukla, A. Krajnc, T. Wang, X. Li, R. Doasa, L. H. G. Tizei, B. Chan, D. N. Johnstone, R. Lin, T. U. Schülli, I. Martens, D. Appadoo, M. S. Ari, Z. Wang, T. Wei, S.-C. Lo, M. Lu, S. Li, E. B. Namdas, G. Mali, A. K. Cheetham, S. M. Collins, V. Chen, L. Wang and T. D. Bennett, *Science*, 2021, **374**, 621–625.
17 D. K. Dalavi, D. P. Bhopate, A. S. Bagawan, A. H. Gore, N. K. Desai, A. A. Kamble, P. G. Mahajan, G. B. Kolekar and S. R. Patil, *Anal. Methods*, 2014, **6**, 6948–6955.
18 A. G. Moiseev, E. A. Margulies, J. A. Schneider, F. Bélanger-Gariépy and D. F. Perepichka, *Dalton Trans.*, 2014, **43**, 2676–2683.
19 H. L. Pradeepa, A. Bid and J. K. Basu, *Nanoscale Adv.*, 2020, **2**, 3858–3864.
20 W. Chen, S. Horike, D. Umeyama, N. Ogiwara, T. Itakura, T. Tassel, Y. Goto, H. Kageyama and S. Kitagawa, *Angew. Chem.*, 2016, **128**, 5281–5286.
21 P. Sannigrahi and E. Ingall, *Geochem. Trans.*, 2005, **6**, 52.
22 T. Watcharatpong, T. Pila, T. Maihom, T. Ogawa, T. Kurihara, K. Ohara, T. Inoue, H. Tabe, Y.-S. Wei, K. Kongpatpanich and S. Horike, *Chem. Sci.*, 2022, **13**, 11422–11426.
23 Y. Yang, C. Zhang, C. Zhang, Y. Shi, J. Li, B. Johannessen, Y. Liang, S. Zhang, Q. Song, H. Zhang, J. Huang, J. Ke, L. Zhang, Q. Song, J. Zeng, Y. Zhang, Z. Geng, P.-S. Wang, Z. Wang, J. Zeng and F. Li, *Nat. Commun.*, 2024, **15**, 6316.
24 A. Shimamura, M. I. Jones and J. B. Metson, *J. Solid State Chem.*, 2022, **316**, 123567.
25 S. Jung, W.-L. Cheung, S.-J. Li, M. Wang, W. Li, C. Wang, X. Song, G. Wei, Q. Song, S. S. Chen, W. Cai, M. Ng, W. K. Tang and M.-C. Tang, *Nat. Commun.*, 2023, **14**, 6481.
26 V. A. Dini, D. Genovese, C. Micheletti, N. Zaccheroni, A. Pucci and C. Gualandi, *Aggregate*, 2023, **4**, e373.
27 Z. Qi, Y. J. Ma and D. Yan, *Aggregate*, 2024, **5**, e411.